Chin. J. Astron. Astrophys. Vol. 6 (2006), No. 6, 641–648
(*http://www.chjaa.org*)

Chinese Journal of
Astronomy and
Astrophysics

Chemical Evolution of Blue Compact Galaxies *

Fei Shi[1,2], Xu Kong[1] and Fu-Zhen Cheng[1]

[1] Center for Astrophysics, University of Science and Technology of China, Hefei 230026
sfemail@mail.ustc.edu.cn
[2] National Astronomical Observatories, Chinese Academy of Sciences, Beijing 100012

Received 2006 February 14; accepted 2006 August 9

Abstract Based on a sample of 72 Blue Compact Galaxies (BCGs) observed with the 2.16 m telescope of the National Astronomical Observatories, Chinese Academy of Sciences (NAOC) and about 4000 strong emission line galaxies from the Sloan Digital Sky Survey, we analyzed their chemical evolution history using the revised chemical evolution model of Larsen et al. Our sample covers a much larger metallicity range ($7.2 < 12 + \log(\mathrm{O/H}) < 9.0$). We found that, in order to reproduce the observed abundance pattern and gas fraction over the whole metallicity range, a relatively continuous star formation history is needed for high metallicity galaxies, while assuming a series of instantaneous bursts with long quiescent periods (some Gyrs) for low metallicity galaxies. Model calculations also show that only the closed-box model is capable of reproducing the observational data over the whole metallicity range. Models that consider the ordinary winds and/or inflow can only fit the observations in the low metallicity range, and a model with enriched wind cannot fit the data in the whole metallicity range. This implies that the current adopted simple wind and inflow models are not applicable to massive galaxies, where the underlying physics of galactic winds or inflow could be more complicated.

Key words: galaxies: abundance — galaxies: evolution — galaxies: starburst — stars: formation

1 INTRODUCTION

Blue compact galaxies (BCGs) are characterized by compact appearance, high gas content, very blue color, and low chemical abundances (Kong & Cheng 2002). The chemical evolution of BCGs is of particular interest because these systems are relatively simple systems, with low level of metal enrichment and absence of large abundance gradients (Larsen et al. 2001). Furthermore, their wide range of intrinsic properties makes them suitable for testing certain expectations from stellar nucleosynthesis theory and models of galactic chemical evolution (Kunth & Östlin 2000).

A large number of theoretical models for BCGs have been proposed (e.g., Matteucci & Chiosi 1983; Pilyugin 1993; Marconi et al. 1994; Carigi et al. 1995; Kunth et al. 1995; Lanfranchi & Matteucci 2003; Izotov & Thuan 2004) to explain their observed abundances and variations and to understand their chemical evolution. Some convergence has been reached regarding their chemical evolution: the initial mass function (IMF) is the same everywhere with a slope similar to the Salpeter (1955) function ($\alpha = -2.35$); galactic winds with varying efficiencies are necessary to explain the observational data; the process of star formation is discontinuous, characterized by short bursts separated by quiescent periods. Larsen et al. (2001) have developed a numerical model of chemical evolution, and found that the model including enriched winds does not give a good fit to the number ratio of nitrogen to oxygen (N/O) (similarly, He/H and O/H will

* Supported by the National Natural Science Foundation of China.

hereafter denote the helium-to-hydrogen and oxygen-to-hydrogen number ratios), whereas closed models, models with ordinary winds, or a combination of ordinary winds and inflow, are all found to be viable.

Recently, we have observed an atlas of high-quality ground-based optical spectra of 97 BCGs (Kong & Cheng 2002) at the 2.16 m telescope at the Xinglong Station of NAOC. The electron temperatures, electron densities, nitrogen abundances, and oxygen abundances for 72 star-forming BCGs in our sample have been determined in Shi et al. (2005). Our sample galaxies have a metallicity range from 7.15 to 9.0. When we applied the models of Larsen et al. (2001) to our sample, we found that the chemical evolution models of Larsen et al. (2001) can fit the observations of low metallicity (dwarf) BCGs ($12 + \log(\mathrm{O/H}) < 8.3$ for Larsen et al.'s sample) well, but their models cannot be used for the high metallicity (massive) galaxies. Because star-forming galaxies of all types in the local universe follow a luminosity-metallicity correlation (e.g., Lequeux et al. 1979; Skillman et al. 1989), objects more luminous than $M_B \sim -18$ have metallicities larger than $12 + \log(\mathrm{O/H}) \sim 8.3$. We regard the galaxies of $12 + \log(\mathrm{O/H}) > 8.3$ as massive galaxies, and the galaxies of $12 + \log(\mathrm{O/H}) < 8.3$ as dwarf galaxies.

One possible reason for this distinction is that the star formation history (SFH) is different for dwarf and massive galaxies. Based on observational data and numerical methods, many research groups found that the SFH of dwarf galaxies is characterized by intermittent bursts, separated by quiescent periods lasting several Gyrs, whereas massive galaxies have relatively continuous SFHs (Dolphin 2000; Grebel 2001; Mouhcine & Contini 2002; Kong et al. 2003). The assumption of SFH in Larsen et al. (2001) works well only for dwarf galaxies.

In this paper, we will revise the chemical evolution model of Larsen et al. (2001), by altering the SFH for massive galaxies, to make it suitable for simulating the chemical evolution history of starburst galaxies in the whole metallicity region.

The paper is organized as follows. Section 2 summarizes the observational constraints for the chemical evolution of starburst galaxies. Section 3 describes our revised chemical evolution model. The results of fitting the models to the sample of observations are presented in Section 4, a discussion and a summary are given in Section 5.

2 OBSERVATIONAL CONSTRAINTS

We have observed the optical spectra of 97 BCGs at the 2.16 m telescope of NAOC (Kong & Cheng 2002). A 300 line mm^{-1} grating was used to achieve coverage in the wavelength region from 3580 to 7400 Å with about 4.8 Å per pixel resolution. The slit width was switched between $2''$ and $3''$ each night, depending on the seeing conditions. The average signal-to-noise ratio of the spectra is ~ 51 per pixel. The fluxes and equivalent widths of emission lines, continuum fluxes, the 4000 Å break, and the equivalent widths of several absorption features were measured in Kong et al. (2002).

Based on the high-quality ground-based spectroscopic observations, Shi et al. (2005) have determined the electron temperatures, electron densities, nitrogen abundances, and oxygen abundances for 72 star-forming BCGs (spectrum with strong emission lines) in our sample, using different oxygen abundance indicators.

The preferred method for determining the oxygen abundance in galaxies is through electron temperature-sensitive lines (the so-called T_e method), such as the [O III] λ4363 line. In this paper, the adopted metallicity of BCGs is determined from T_e method.

In order to enlarge the observed sample, we have added emission line galaxies from the Third Data Release (DR3) of the Sloan Digital Sky Survey (SDSS). SDSS is the most ambitious imaging and spectroscopic survey to date, and will eventually cover a quarter of the sky and observe 180 million individual objects (York et al. 2000). The SDSS-DR3 spectroscopic data include data from 826 plates of 640 spectra each, and have 374, 767 spectra of galaxies.

After subtracting the underlying starlight using the method of Li et al. (2005) and Lu et al. (2006), we fit the emission line using the method of Dong et al. (2005). Then, two subsamples were selected from the SDSS-DR3, on the criterion that the [O II] λ3727, Hβ λ4861, [O III] λ4959, [O III] λ5007, Hα λ6563 and [N II] λ6583 all have fluxes more than 5 times their uncertainty. The difference of these two subsamples is that Sample I is selected by the additional criterion on the [O III] λ4363 line, that the flux of this line is more than 5σ. Now, [O III] λ4363 is strongly dependent on the metallicity of the galaxy, being undetectable in high metallicity galaxies. So the galaxies in Sample I are low metallicity galaxies. There are 225 galaxies in

Sample I. The electron temperature of galaxies in Sample I was calculated from this temperature-sensitive line, [O III] λ4363. In Sample II, the galaxies have weak [O III] λ4363 lines, but the signal-to-noise of the other strong emission lines are higher than 5, and there are 3997 galaxies in Sample II. The electron temperature of galaxies in Sample II was calculated by an empirical method. A detailed description of the sample selection, the electron temperatures, electron densities, nitrogen abundances, and oxygen abundances calculation are given in Shi et al. (2006).

Systematic difference between these two samples is important to our results. Because no match has been found between the BCG sample and the SDSS sample, it is difficult to discuss the systematic difference in detail. Since galaxies in both samples have undergone the same process of subtraction of underlying stellar absorption and of correction of internal reddening, however, one possible systematic difference between these two samples might come from difference in the observing aperture or in the observed position of the galaxy. We will discuss this in detail in a forthcoming paper when matching objects are found between our BCG sample and the new data release of SDSS.

A feasible model must simulate all the observations at the same time. Besides the relation of N/O vs. O/H, the dependence on O/H of the helium mass function, He/H, and the fractional mass of gas, $\mu = M_{\rm gas}/M_{\rm tot}$, are also used to constrain the chemical evolution model. The helium mass function is taken from Izotov et al. (1998), and the fractional mass of gas is taken from Larsen et al. (2001).

3 THE MODEL

In an effort to understand the chemical evolution of gas-rich dwarf galaxies, Larsen et al. (2001) developed a numerical model of chemical evolution, which allows one to follow in detail the evolution of the abundances of several elements, starting from the matter reprocessed by the stars and restored into the interstellar medium (ISM) by winds and type II supernova (SNII) explosions. The main features of the model are as follows, further details can be found in Larsen et al. (2001):

- a one-zone description with instantaneous mixing was assumed;
- to account for scatter in N/O, the bursts are assumed to be instantaneous and ordered in pairs;
- the Salpeter IMF was used, with $\alpha = -2.35$, $m_{\rm U} = 100\,M_{\odot}$, and $m_{\rm L} = 0.1, 0.05$ or $0.01\,M_{\odot}$;
- no instantaneous recycling approximations, i.e. the stellar lifetimes are taken into account;
- closed model with consideration of enriched winds, ordinary winds, and inflow.
- four sets of theoretical yields are used (see detail in table 2 of Larsen et al. 2001):
  set 1. massive stars: Maeder (1992) and Woosley & Weaver (1995); intermediate mass stars: van den Hoek & Groenewegen (1997).
  set 2a. massive stars: as in set 1; intermediate-mass stars: Renzini & Voli (1981).
  set 2b. as for 2a; but with lower mass loss above 9 $M_{\odot}$.
  set 3. massive stars: Portinari et al. (1998); intermediate and low-mass stars: Marigo et al. (1996, 1998).

As a first test calculation, we applied the above model to our sample, and the results are plotted in Figure 1. The figure shows that the Larsen models can be used only in the low metallicity region. When it was applied to the high metallicity region (of mostly massive galaxies), there was considerable deviation from the observations. The main reason for the deviation is that the adopted SFH in Larsen et al. (2001) is not suitable for massive galaxies.

As mentioned in the introduction, many research groups found the star formation histories of dwarf galaxies and massive galaxies to be different. It is necessary to revise the SFH for massive galaxies. In the low [O/H] region, our adopted SFH is the same as Larsen et al. (2001), that is, the very first burst is a single one, all the others appearing in pairs. The inter-burst period within a pair is tuned to give maximum scatter in N/O, which turns out to be 30 Myr. The time between pairs is set to be 1 Gyr. In the high metallicity region after some tests we found that the results from a relatively continuous star formation history can fit the observational data. Therefore, a 30 Myr quiescent period between each pairs was used. We also discussed the results by adopting a model of continuous star formation history for massive galaxies. The age of the galaxy in all the calculations were assumed to be 15 Gyr.

The IMF $\phi(M)$ specifies the mass distribution in a newly formed stellar population and it is frequently assumed to be a simple power law $\phi(M) = \phi_0 M^{-\alpha}$. The slope α determines the mass distribution of

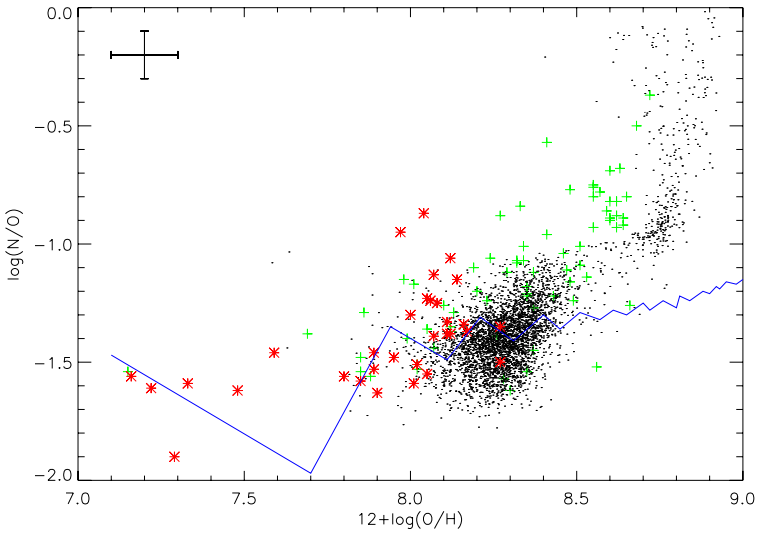

Fig. 1 Evolution of N/O ratio for a closed model from Larsen et al. (2001) (fig. 6, in their paper). The solid line shows the evolutionary path, calculated by the model; stars are galaxies used in Larsen et al. (2001); the plus signs are 72 BCGs in Shi et al. (2005); and the dots are galaxies from SDSS (Shi et al. 2006). Typical systematic error bars for the two samples are marked at upper left.

stars, and stars of different masses generate different ranges of chemical elements, therefore, the chemical abundances and their ratios are extremely sensitive to the initial mass function. Thus, we made model calculations for both the Salpeter IMF (single power law) and the Kroupa et al. (2001) IMF (multiple power law).

4 RESULTS

We apply the models described in Section 3 to fit the observational relations, N/O vs. O/H, He/H vs. O/H and gas fraction (μ) vs. O/H, with the same input parameters. In this section, we will mainly discuss the closed model.

All of the stellar yield sets are studied for the closed model. Other free parameters in the model include: burst mass and low-mass cut off in the adopted IMF.

As already demonstrated in Larsen et al.(2001), the level of N/O is much too high, in particular at low metallicities, if the yield set 1 is used. The real problem for this set is that the yield from van den Hoek & Groenewegen (1997) does not distinguish between primary and secondary components. Thus, it is not possible to scale the secondary components separately to $Z = 0$. Therefore, we do not study yield set 1 in detail in this paper.

In Figure 2, the solid line shows the calculated evolutionary path using yield set 2a and the Salpeter IMF. The total mass of the galaxy and the mass of burst adopted in the model calculations are $10^8\,M_\odot$ and $3\times10^6\,M_\odot$, respectively. The left panels of Figure 2 show the results for a closed model, with $m_{\rm L}$= $0.1\,M_\odot$. From this figure, we find that the model with the revised star formation histories fit all the observational constrains well, with the same input parameters.

A similar run is presented in the right panels of Figure 2 for $m_{\rm L} = 0.01$ and $0.05\,M_\odot$. The lower-mass cut-off is an important parameter because the yield from a generation of stars is a function of the adopted lower mass limit. The reason is that stars less massive than $\sim 1\,M_\odot$ do not eject metals, thus locking up all the material from which they are formed. Hence, lowering the lower mass cut-off implies a lower recycling fraction, giving a lower yield: the yield will be a factor of 2–3 lower when using the lower cut-off. As expected, the results shown in the left and right panels of Figure 2 are different. For example, (He/H) vs.

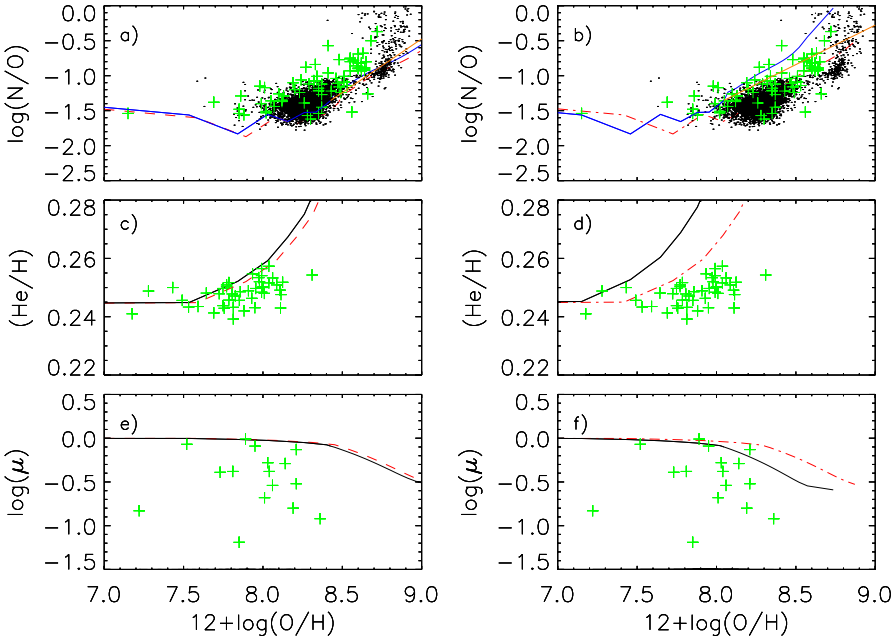

Fig. 2 Results for a closed model with yield set 2a and $m_{\rm L}$=0.1 $M_{\odot}$ (left panels) and $m_{\rm L}$=0.01 $M_{\odot}$ (solid lines), 0.05 $M_{\odot}$ (dot-dashed lines) (right panels). Dashed lines for IMF from Kroupa (2001), blue solid lines for IMF from Salpeter (1955), orange solid lines for the continuous star formation history for high metallicity galaxies. The observations shown are the same as in Fig. 1 for N/O and $12 + \log(\mathrm{O/H})$; the helium mass function, (He/H), is from Izotov et al. (1998); and the gas fraction, μ, is from Larsen et al. (2001).

$12 + \log(\mathrm{O/H})$ does not fit well the result of Salpeter IMF with $m_{\rm L} = 0.01\,M_{\odot}$ in the right panel. The result of Salpeter IMF with $m_{\rm L} = 0.05\,M_{\odot}$ (which is between those of $m_{\rm L} = 0.01$ and $m_{\rm L} = 0.1\,M_{\odot}$) fits better. If in the model with $m_{\rm L} = 0.01$ of Figure 2 we change all its bursts in SFH to twice the burst mass ($6 \times 10^6\,M_{\odot}$), then the behaviours of $m_{\rm L} = 0.01$ and $m_{\rm L} = 0.1\,M_{\odot}$ in Figure 2 will be quite similar.

The dashed lines in the left panels of Figure 2 show the results for a closed model, calculated for the yield set 2a and the Kroupa (2001) IMF with $m_{\rm L}$= 0.1 $M_{\odot}$. This figure shows that the result of the Kroupa IMF and the Salpeter IMF are similar, with a very small systematic difference between them. Thus, the chemical evolution seems to be insensitive to the slope of the IMF.

The orange solid lines are the model results for the definitely continuous burst of star formation for high metallicity galaxies. We assume the star formation rate remains constant ($0.6 \times 10^{-2}\,M_{\odot}$ yr^{-1}) in the last 1 Gyr. It is obvious that the closed model with the definitely continuous burst star formation is suitable to fit the observations in the high metallicity region. The systematic difference between the definitely continuous burst of star formation and the relatively continuous burst of star formation is negligible.

Figure 3a shows the evolutionary paths for different fractional burst masses. All of the parameters, except the mass of each burst, are the same as for the right panels of Figure 2: a closed model, for yield set 2a, Salpeter IMF and $m_{\rm L}$= 0.1 $M_{\odot}$. The dashed line, the solid line and the dot-dashed line correspond to burst masses equal to 1%, 3% and 5% of the total mass of the galaxy, respectively. In the low metallicity region, the time interval between two pairs of bursts is $\sim$ 1 Gyr, enough to release almost all of the nitrogen. Thus, larger burst mass increase both N and O, so roughly, it does not change N/O. In the high metallicity region, because the time interval between two pairs of bursts is very short, the N from the pair-burst has not yet been released in this short time. Thus, a larger burst mass gives an increase only in the O abundance, making the level of N/O of the burst lower. Two additional results may be deduced from Figure 3a. First, the scatter of the observations in whole metallicity region can be explained easily, by models of BCGs

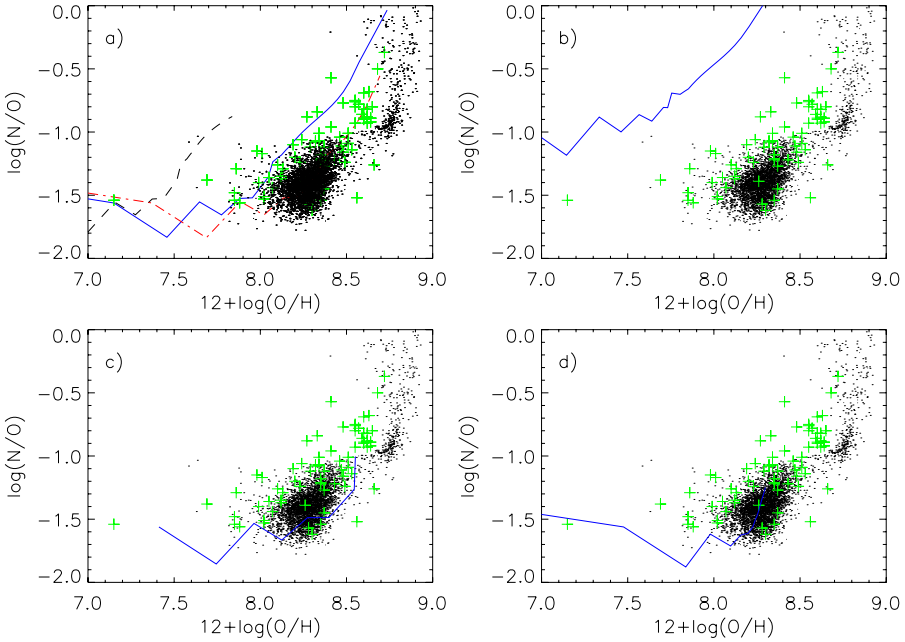

Fig. 3 N/O ratio as a function of the oxygen abundance, using the yield set 2a, Salpeter IMF and $m_{\rm L}$= $0.01\,M_{\odot}$. The observations shown are the same as in Fig. 1. a) for three closed models, with different burst masses: the dashed line, solid line and dot-dashed line correspond to burst masses of 1%, 3% and 5% of the total mass of the galaxy. b) Results of models with metal-enhanced winds. c) Results of using a model including ordinary winds. d) Results of using a model including both inflow and ordinary winds.

having various relative burst masses over a reasonable range. Furthermore, besides giving a good fit to the observational data in the low metallicity region, the revised model gives a better fit to the high metallicity region, than does the original model of Larsen et al. (2001).

Yield set 2b is different from yield set 2a only in that a modest mass-loss from massive stars is assumed. Yield set 3 is from the Padova tracks, and yield set 2, from the Geneva tracks. However, as already demonstrated in Larsen et al. (2001), the behavior of yield set 3, set 2a and set 2b are quite similar. Therefore, we do not repeat the calculations with these yields in this paper, and draw the conclusion that yield sets 2a, 2b and 3 are suitable stellar yields for modeling the chemical evolution. Adoption of different yield sets does not change the results significantly. It is worth emphasizing that the helium abundances and gas fraction are fitted with the same input parameters as used to fit the N/O ratio. It is clear that the closed model fits well with the results of observation of BCGs.

5 DISCUSSION AND SUMMARY

Using a sample of 72 BCGs and about 4000 SDSS strong emission line galaxies, we analyzed the chemical evolution in BCGs, comparing He, N/O, μ to the detailed predictions of the chemical evolution models. By taking into account the IMF slope, the low-mass cutoff $m_{\rm L}$ of IMF, the stellar yields, the closed model or open models, we followed the evolution of several chemical elements and gas fraction. The main conclusions can be summarized as follows.

If we want to have a good model fit to the observation of BCGs over the whole metallicity region, the SFH in the original model of Larsen et al. (2001) has to be revised: we need to have a relatively continuous star formation history for high metallicity galaxies, and a series of instantaneous bursts with long quiescent period (some Gyrs) in between for low metallicity galaxies. Our revised closed models (with different star formation histories) can fit the evolution of abundance and gas fraction over the whole metallicity region, while the original Larsen et al.'s (2001) model can only fit the observational data in the low metallicity

region. These results support the idea that the SFH is an important parameter and that massive galaxies have a relatively continuous star formation history.

Besides the closed model, we also discussed the model including inflow and outflow. Figure 3b shows the results of including enriched winds. The model is applied to fit the observations in the log(N/O)–$12 + \log(\mathrm{O/H})$ plane, with the yield set 2a. Since enriched wind is caused by SNII, and oxygen dominates the ejecta from SNII, the winds will improve the efficiency of oxygen removal. The removal efficiency of oxygen is determined, by fitting the gas fractions, to be equal to 0.8, which means that 80% of the ejected mass of oxygen is expelled from the galaxy. Using our model with the revised star formation histories, we found that the upturn in the high metallicity region in our model is steeper than that in Larsen et al. (2001). Removing much oxygen increases the N/O ratio dramatically above the level of observations, as seen in Larsen et al. (2001) and Figure 3b of this paper. Although the behaviour of the revised model including enriched winds and that of the original Larsen et al. (2001) are different, the result is very similar. Hence, a model including enriched winds can not fit the observations in the log(N/O)–$12 + \log(\mathrm{O/H})$ plane, neither explain the chemical evolution history over the whole metallicity range.

The other possibility of outflow is ordinary galactic winds, which arises from a general heating of the ISM, causing a fraction to leave the galaxy, in this case the gas leaving the galaxy has the same composition as the ISM. As in Larsen et al. (2001), we suppose the mass loss by ordinary wind to be 5 times the burst mass. By multiplying the mass of the wind with the fraction of the same kind of element (C, N, O, or He) in the ISM, taken just before the burst that is responsible for the wind, we obtain the mass removed of the particular element due to an ordinary wind. Figure 3c shows the results of including ordinary winds, with the yield set 2a. The figure shows that a mass removal of 5 times the burst mass does not appreciably change the behaviors from the closed model in the low metallicity range. The model including ordinary winds cannot evolve to high metallicity region. The behavior of our ordinary wind model is similar to that of Larsen et al. (2001). Both models can be used to explain the N/O –O/H relation of low metallicity galaxies, but it is impossible to bring the evolutionary path to the N/O – O/H relation of high metallicity galaxies. Because most of high metallicity galaxies are massive galaxies with high gravity, parts or all of the outflow will return back to the galaxy. This feedback effect makes the chemical evolution model more complex and our simple ordinary wind model does not agree with the observation in the high metallicity region.

The model including inflow is also important for understanding the chemical evolution history of the galaxy. Inflow means increase in the galaxy mass, the inflow rate is given by $\dot{M}(t) = (M_0 \times e^{-t/\tau_{\rm inf}})/\tau_{\rm inf}$ (Lacey & Fall 1985). Two new parameters are needed: the total mass accreted onto the galaxy M_0 and the duration of the inflow event $\tau_{\rm inf}$. Using the same parameters as Larsen et al. (2001), we ran the model including ordinary winds and inflow, and the resulting evolutionary path of N/O – O/H is shown in Figure 3d. From the figure it can be seen that this model fits the observation well only in the low metallicity region, but not in the high metallicity region, as the model not including inflow. The model including both ordinary winds and inflow cannot fit well with the observation in the whole metallicity region.

Our revised (star formation history) closed model fits the observation well over the whole metallicity region, but there are still limitations: the model cannot explain the scatter in the N/O, He/H, μ vs. O/H plots. A more complex star forming history and a varying fraction of burst mass may account for to these scatters.

In addition, we also considered the effects of the IMF slope, the low-mass cutoff $m_{\rm L}$ of IMF, the stellar yields, and the fraction of burst mass. We found that the slope of IMF (Kroupa 2001; Salpeter 1995) has little effect on the model outputs, but the low-mass cutoff $m_{\rm L}$ of IMF is an important parameter. Four different stellar yields were used. Except for the yield set 1, which does not distinguish between primary and second components effects, the other sets, 2a, 2b and 3 all fit well the observations and can simulate the chemical evolution history of the galaxies. The changes of burst mass (for an example, 1%, 3%, or 5%) are very important to explain the scatter in the relation between N/O and O/H, and the other relations.

Acknowledgements This work is based on observations made with the 2.16 m telescope of the National Astronomical Observatories, CAS, and is supported by the National Natural Science Foundation of China (Nos. 10573014 and 10633020). The referee, J. L. Hou, and two other anonymous referees are thanked for their constructive report, which helped improve the paper. We are grateful to the AGN group at the Center for Astrophysics, University of Science of Technology of China for processing the SDSS spectra for continuum decomposition and line fitting using the spectral analysis algorithm developed by the group. Funding for the

Sloan Digital Sky Survey (SDSS) has been provided by the Alfred P. Sloan Foundation, the Participating Institutions, the National Aeronautics and Space Administration, the National Science Foundation, the U.S. Department of Energy, the Japanese Monbukagakusho, and the Max Planck Society. The SDSS Web site is *http://www.sdss.org/*. The SDSS is managed by the Astrophysical Research Consortium (ARC) for the Participating Institutions. The Participating Institutions are The University of Chicago, Fermilab, the Institute for Advanced Study, the Japan Participation Group, The Johns Hopkins University, the Korean Scientist Group, Los Alamos National Laboratory, the Max-Planck-Institute for Astronomy (MPIA), the Max-Planck-Institute for Astrophysics (MPA), New Mexico State University, University of Pittsburgh, University of Portsmouth, Princeton University, the United States Naval Observatory, and the University of Washington.

References

Carigi L., Colin P., Peimbert M., Sarmiento A., 1995, ApJ, 445, 98
Dolphin A. E., 2000, MNRAS, 313, 281
Dong X.-B., Zhou H.-Y., Wang T.-G. et al., 2005, ApJ, 620, 629
Grebel E. K., 2001, Ap&SS, 277, 231
Izotov Y. I., Thuan T. X., 1998, ApJ, 500, 188
Izotov Y. I., Thuan T. X., 2004, ApJ, 602, 200
Kong X., Cheng F. Z., 2002, A&A, 389, 845
Kong X., Cheng F. Z., Weiss A. et al., 2002, A&A, 396, 503
Kong X., Charlot S., Weiss A., Cheng F. Z., 2003, A&A, 403, 877
Kroupa P., 2001, MNRAS, 322, 231
Kunth D., Matteucci F., Marconi G., 1995, A&A, 297, 634
Kunth D., Östlin G., 2000, A&A Rev., 10, 1
Lacey C. G., Fall S. M., 1985, ApJ, 290, 154
Lanfranchi G. A., Matteucci F., 2003, MNRAS, 345, 71
Larsen T. I., Sommer-Larsen J., Pagel B. E. J., 2001, MNRAS, 323, 555
Lequeux J., Peimbert M., Rayo J. F. et al., 1979, A&A, 80, 155
Li C., et al., 2005, AJ, 129, 669
Lu H., Zhou H., Wang J. et al., 2006, AJ, 131, 790
Maeder A., 1992, A&A, 264, 105
Marconi G., Matteucci F., Tosi M., 1994, MNRAS, 270, 35
Marigo P., Bressan A., Chiosi C., 1996, A&A, 313, 545
Marigo P., Bressan A., Chiosi C., 1998, A&A, 331, 564
Matteucci F., Chiosi C., 1983, A&A, 123, 121
Mouhcine M., Contini T., 2002, A&A, 389, 106
Pilyugin L. S., 1993, A&A, 277, 42
Portinari L., Chiosi C., Bressan A., 1998, A&A, 334, 505
Renzini A., Voli M., 1981, A&A, 94, 175
Salpeter E. E., 1955, ApJ, 121, 161
Shi F., Kong X., Li C., Cheng F. Z., 2005, A&A, 437, 849
Shi, F., Kong, X., & Cheng F. Z., 2006, A&A, 453, 487
Skillman, E. D., Kennicutt R. C., Hodge P. W., 1989, ApJ, 347, 875
van den Hoek L. B., Groenewegen M. A. T., 1997, A&AS, 123, 305
Woosley S. E., Weaver T. A., 1995, ApJS, 101, 181
York D. G. et al., 2000, AJ, 120, 1579